CCVD Synthesis and Characterization of Cobalt-Encapsulated Nanoparticles

E. Flahaut,*,† F. Agnoli,‡ J. Sloan,† C. O'Connor,‡ and M. L. H. Green†

Wolfson Catalysis Centre (Carbon Nanotechnology Group), Inorganic Chemistry Laboratory, University of Oxford, South Parks Road, Oxford OX1 3QR, U.K.; and Advanced Materials Research Institute, College of Science, University of New Orleans, 2000 Lakeshore Drive, New Orleans, Louisiana 70148

Received November 26, 2001. Revised Manuscript Received February 13, 2002

Cobalt nanoparticles encapsulated in carbon shells have been synthesized by catalytic chemical vapor deposition (CCVD) in high yield by reducing with a H_2/CH_4 gas mixture a $Mg_{0.9}Co_{0.1}O$ solid solution impregnated MgO (SSI−MgO) catalyst. The carbon-encapsulated Co nanoparticles have a narrow distribution of diameters within the range 5−15 nm. They are made of (fcc)-Co as shown by XRD and are very stable to air oxidation; the magnetic properties have been investigated using a SQUID magnetometer and confirm that Co is present in the metallic state.

Introduction

The synthesis of metal carbon-encapsulated nanoparticles has attracted much attention[1] for their technological promise, in particular as magnetic materials with potential applications in data storage.[2] However, the high surface-to-volume ratio of metal nanoparticles leads to their rapid oxidation, and therefore, an efficient oxidation-resistant coating is required. One candidate for such a material is carbon-encapsulated magnetic-metal nanoparticles. These have been produced by carbon arc methods involving the evaporation of a metal-doped graphite anode in an inert atmosphere.[3,4] This arc synthesis method produces the encapsulated nanoparticles together with sootlike material, including carbon nanotubes and graphitic particles, which makes their purification and separation difficult. However, some modifications of the traditional arc process can allow for the preparation of controlled-size graphite-encapsulated metal particles.[5] Recent attempts to synthesize ferromagnetic metal nanocrystals has included the preparation of pure and well-crystallized Ni nanoparticles[6] by thermal decomposition in Ar of the organometallic compound $Ni(COD)_2$. These Ni nanoparticles were formed as a dispersion in an amorphous carbon matrix, and their diameter distribution was found to be bimodal (2−5 and 10−20 nm). Recent preparations of Fe nanoparticles gave either particles of diameter ca. 70 nm[7] or particles with a large diameter distribution (10−100 nm).[8] In both cases, the Fe particles were mainly located at the end of short and defect-containing carbon nanotubes. The preparation of Co nanoparticles by plasma arcing[9] has been described recently, but the particles formed within the 10−50 nm diameter range were embedded in amorphous carbon. Carbon-coated Co nanoparticles have been formed via a solid-state reaction involving the heat treatment, up to 1700 °C, of a mixture of Co nanoparticles and diamond.[10] This procedure gave carbon-encapsulated Co nanoparticles of diameter ca. 60 nm.

Here we report the preparation of very small Co nanoparticles encapsulated in graphitised carbon shells. We have used a CCVD method involving the reduction by a H_2/CH_4 mixture of a $Mg_{1-x}Co_xO$ solid solution[11] prepared by the combustion method.[12] $Mg_{1-x}Co_xO$ solid solutions have been successfully prepared and used for the synthesis of carbon nanotubes,[11,13] but we show here that control of the experimental conditions can favor either the formation of carbon nanotubes or the formation of encapsulated nanoparticles. To enhance the efficiency of the $Mg_{1-x}Co_xO$ solid solution, we have

* Corresponding author. Present address: CIRIMAT/LCMIE−UMR CNRS 5080, Université Paul Sabatier, 118 Route de Narbonne, 31062 Toulouse Cedex 4, France. Telephone: +33-561556970. Fax: +33-561556163. E-mail: flahaut@chimie.ups-tlse.fr.

† University of Oxford.

‡ University of New Orleans.

(1) Subramoney, S. *Adv. Mater.* **1998**, *10*, 1157.
(2) McHenry, M. E.; Majestich, S. A.; Kirkpatrick, E. M. *Mater. Sci. Eng.* **1995**, *204*, 19.
(3) Saito, Y. *Carbon* **1995**, *33*, 979.
(4) Jiao, J.; Seraphin, S. *J. Appl. Phys.* **1997**, *83*, 2442.
(5) Dravid, V. P.; Host, J. J.; Teng, M. H.; Elliot, B.; Hwang, J.; Johnson, D. L.; Mason, T. O.; Weertman, J. R. *Nature (London)* **1995**, *374*, 602.
(6) Rojas, T. C.; Sayagués, M. J.; Caballero, A.; Koltypin, Y.; Gedanken, A.; Ponsonnet, L.; Vacher, B.; Martin, J. M.; Fernández, A. *J. Mater. Chem.* **2000**, *10*, 715.
(7) Zhang, X. X.; Wen, G. W.; Huang, S.; Dai, L.; Gao, R.; Wang, Z. L. *J. Magn. Magn. Mater.* **2001**, *231*, 9.
(8) Liu, S.; Tang, X.; Mastai, Y.; Felner, I.; Gedanken, A. *J. Mater. Chem.* **2000**, *10*, 2502.
(9) Kalman, J.; Nordlund, C.; Patney, H. K.; Evans, L. A.; Wilson, M. A. *Carbon* **2001**, *39*, 137.
(10) Tomita, S.; Hikita, M.; Fujii, M.; Hayashi, S.; Akamatsu, K.; Deki, S.; Yasuda, H. *J. Appl. Phys.* **2000**, *88*, 5452.
(11) Flahaut, E.; Peigney, A.; Laurent, Ch.; Rousset, A. *J. Mater. Chem.* **2000**, *10*, 249.
(12) Patil, K. C. *Bull. Mater. Sci.* **1993**, *16*, 533.
(13) Bacsa, R. R.; Laurent, Ch.; Peigney, A.; Bacsa, W. S.; Vaugien, Th.; Rousset, A. *Chem. Phys. Lett.* **2000**, *323*, 566.

10.1021/cm011287h CCC: $22.00
Published on Web 04/23/2002

designed a new preparation method allowing for the synthesis of a MgO-supported $Mg_{0.9}Co_{0.1}O$ solid solution, as detailed in the Experimental Section. Because the reaction between the solid solution and the reducing H_2-CH_4 gas atmosphere occurs mainly on the surface, a MgO grain coated with a $Mg_{0.9}Co_{0.1}O$ solid solution will yield the same amount of active Co nanoparticles as a pure $Mg_{0.9}Co_{0.1}O$ particle; in this way, the yield of nanoparticles from the available Co is increased.

Experimental Section

To prepare a solid solution impregnated MgO powder (SSI−MgO) containing 70 wt % of MgO, the required weight of MgO (purity >98%, supplied by Aldrich) was mixed with an aqueous solution of $Mg(NO_3)_2 \cdot 6H_2O$, $Co(NO_3)_2 \cdot 6H_2O$ and urea (all supplied by Aldrich, purity >99%) in stoichiometric amounts, as described.[11] The composition of the solution was calculated to correspond to a $Mg_{0.9}Co_{0.1}O$ solid solution. MgO powder was slowly added to the stirred solution and the suspension was allowed to stir for 30 min. The violet suspension obtained was placed in a quartz boat and introduced in an open furnace preheated at 650 °C (in air) and then left until completion of the combustion reaction. Typically, the reaction was over in 5 min. The fluffy solid obtained was then gently ground using a mortar and pestle and stored in an oven at 110 °C prior to utilization. About 10 g of the SSI−MgO was placed in a quartz tube centered inside a tubular furnace which was arranged in vertical position. The SSI−MgO was supported by a quartz frit, so that no reaction boat was necessary. The reactor was arranged in such a way that the powder was exactly in the central hot zone of the furnace, and both ends of the furnace were plugged with silica wool to avoid excessive heat loss. A H_2/CH_4 mixture (18 mol % of CH_4) was flowed into the top of the reactor (i.e. opposite to the frit) at 0.25 L/min while the furnace was heated to 600 °C at 10 °C/min. At this stage, the flow rate was reduced to ca. 50 mL/min. After a temperature of 800 °C was reached, the heating ramp was then adjusted to 5 °C/min. After 1000 °C was reached, the H_2/CH_4 flow was replaced by Ar and the furnace was allowed to cool. The C−Co−MgO product was obtained as a powder: this is in contrast to the CNTs synthesis conditions[11] where the C−Co−MgO product is generally obtained in a lump form keeping the shape of the reaction boat. The C−Co−MgO product was then treated with concentrated HCl[11] to dissolve the MgO support, the unreacted $Mg_{0.9}Co_{0.1}O$ solid solution and non-carbon-coated Co nanoparticles. Typically, 90 mL of a concentrated commercial HCl solution (15 M) was added to 6 g of the C−Co−MgO composite powder and the mixture was sonicated for 15 min before being stirred for 72 h. The resulting black solid was suspended in a Co(II) blue solution; it was separated and washed with deionized water on a 0.4 μm polycarbonate membrane using a Millipore filtration rig and then dried in air at 110 °C. This yielded 140 mg of black solid, which corresponds to a yield of ca. 7.5 wt % with respect to the starting SSI−MgO. Taking into account that the SSI−MgO contained only 30 wt % of $Mg_{0.9}Co_{0.1}O$ solid solution, this represents a yield of ca. 55 wt % with respect to the Co.

X-ray diffraction (XRD) patterns of the C−Co samples were recorded using a Philips PW1710 X-ray diffractometer equipped with a Cu Kα X-ray source. The product was examined using both a JEOL 2000FX transmission electron microscope (TEM) operated at 200 kV and for high-resolution imaging, with a JEOL 3000F field emission gun TEM (FEGTEM) operated at 300 kV, with a spherical aberration coefficient (Cs) of 0.57 and a point resolution of 0.16 nm. Energy-dispersive X-ray microanalysis (EDX) was performed with an Oxford Instruments ISIS 300 system equipped with a LINK "pentafet" detector. A Gatan imaging filter (GIF) equipped with a 2K 794IF/20 Mega Scan CCD was used to obtain elemental maps of the sample. Static magnetic susceptibilities were measured with a Quantum Design MPMS-5S SQUID magnetometer in the temperature range 10−300 K and with field up to 50 kOe.

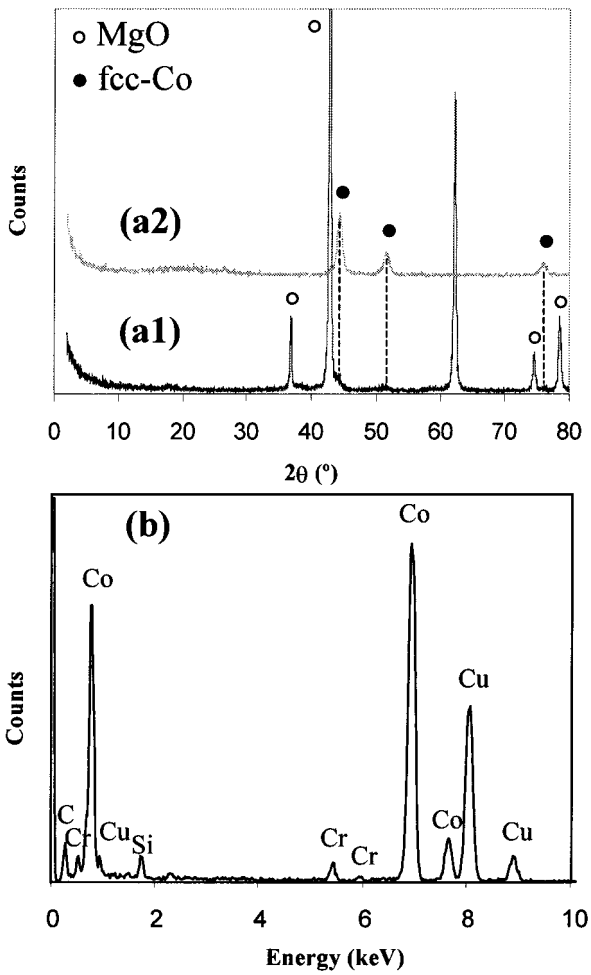

Figure 1. (a) XRD patterns of the C−Co−MgO composite powder (a1) and the black C−Co material obtained after HCl treatment (a2). (b) EDX spectra of the carbon-encapsulated nanoparticles.

Results and Discussion

A comparison between the XRD pattern (Figure 1a1) of the initial C−Co−MgO composite powder and of C−Co particles (Figure 1a2) shows that all the oxide material has been successfully removed. This was further confirmed by EDX, and the only elements we could detect from ca. 20 scans obtained at random from the sample were Co and C (Figure 1b), the other elements coming from the Cu support grid. XRD and electron diffraction studies showed that the black C−Co material contained (fcc)-Co particles and the very low intensity peak observed at 3.34 Å corresponds to graphite-like carbon, although its presence is made difficult to detect because of the small particle size. No carbide Co_3C phase was detected, in agreement with Jiao et al.,[4] but it is difficult to completely rule out the presence of carbide from the XRD pattern because of the very small particle size. Similarly, no (hcp)-Co has been detected, but its presence as a minor constituent is difficult to rule out for the same reason.

The elemental analysis shown that the black C−Co solid contained 27 wt % of carbon, and this was confirmed by TGA analysis, carried out in a flow of air. The TGA data (not shown) indicated that the sample was not oxidized below 300 °C; at that temperature, there was simultaneous oxidation of the carbon (to

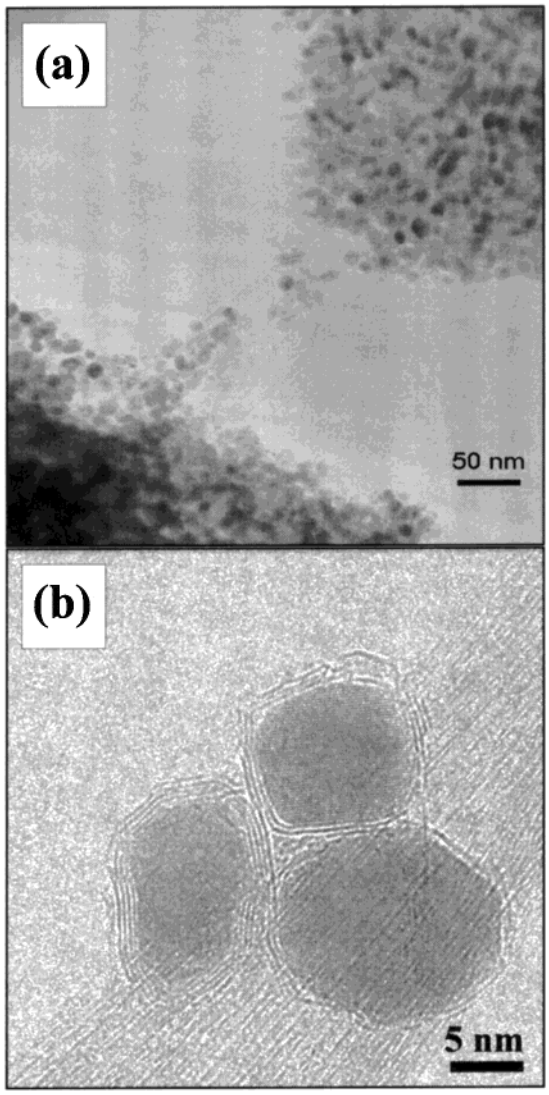

Figure 2. (a) Low-magnification TEM image of the carbon-encapsulated Co nanoparticles after HCl washing of the C−Co−MgO composite powder. The average nanoparticle diameter is between 8 and 9 nm; some particles may be observed to be supported on a bundle of CNTs. (b) HRTEM image of carbon-encapsulated Co nanoparticles supported on a SWNTs bundle. Lattice fringes corresponding to (fcc)-Co metal can be clearly seen within the top particle.

gaseous carbon oxides) and the Co to the oxide Co_3O_4 (XRD); complete oxidation was achieved at ca. 430 °C. A weight loss occurred around 930 °C, because of the transformation of Co_3O_4 into CoO, and this was used to estimate the carbon content in the starting material, assuming that the sample was containing only the elements C and Co. The data gave 28 wt % of C in the black C−Co solid, in good agreement with the elemental analysis, thus confirming that the material contained only C and Co. Also, the selected area electron diffraction patterns of selected encapsulated Co nanoparticles revealed only the spots corresponding to metallic (fcc)-Co.

The observation of the C−Co sample by FEGTEM (Figure 2) showed that it was composed lonely of spheroidal encapsulated Co nanoparticles. The nanoparticle diameters ranged from 4 to 15 nm with most of them falling within a smaller range of between 8 and 9 nm (TEM). The particles were protected from the HCl

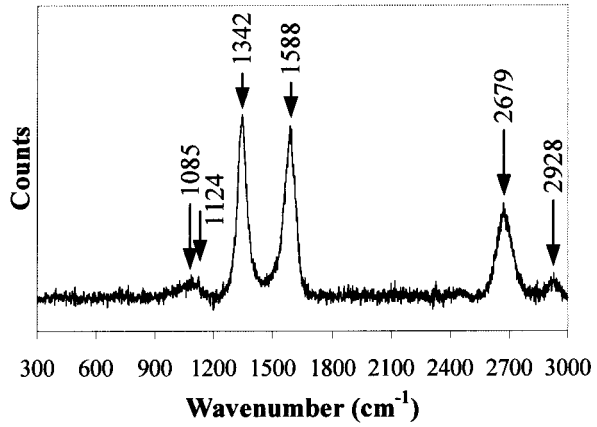

Figure 3. Raman spectra of the carbon-encapsulated Co nanoparticles. The ∼1:1 ratio between the D peak (1342 cm^{-1}) and the G peak (1588 cm^{-1}) suggests the presence of a large amount of sp^3-like carbon, in good agreement with the numerous defects observed by HRTEM in the encapsulating carbon layers.

treatment by the surrounding graphitic shells. The number of concentric carbon shells generally ranged between 2 and 16, with a median of five layers. There was found to be no obvious correlation between the number of graphitic shells and the particle size. No Co nanoparticle encapsulated by single carbon shells was observed. The graphitic shells tightly surrounded the metal nanoparticles and no voids were observed between the metal particle and the first encapsulating graphene layer. A small number of single-walled carbon nanotubes (SWNT) were also observed in the product, usually with a diameter of around 1.5 nm. A few multiwalled carbon nanotubes (diameter between 3 and 4 nm) with straight parallel walls were also occasionally observed.

The black C−Co solid was also studied by Raman spectroscopy and was found to exhibit a strong fluorescence, probably due to the presence of excess Co. For this reason, the sample was submitted to a further purification process consisting of heating it (sealed in a vacuum in a silica ampule) at 1100 °C for 1 h, and then washing it with a concentrated HCl aqueous solution for 12 h. This second washing removed some of the excess Co, as indicated by the blue color of the resulting HCl solution at the end of the operation. Figure 3 shows a typical Raman spectra of the Co encapsulated nanoparticles, characterized by two main peaks centered at 1342 cm^{-1} (D peak) and 1588 cm^{-1} (G peak). The G peak is associated with the E_{2g} mode (stretching vibrations) in the basal-plane of graphite.[14] Broad Raman peaks around 1344 cm^{-1} were observed in disordered graphite[15] as in nanocrystalline graphite and carbon nanotubes.[16,17] The ratio of the D peak to the G peak is known to be inversely proportional to the crystallite size.[15,18] According to Tuinstra et al.,[18] the observed ∼1:1 ratio between the D and G peaks would correspond to a particle size in the 4−5 nm range. This small particle

(14) Nemanich, R. J.; Solin, S. A. *Phys. Rev. B* **1979**, *20*, 392.
(15) Knight, D. S.; White, W. B. *J. Mater. Res.* **1989**, *4*, 385.
(16) Kastner, J.; Picler, T.; Kuzmany, H.; Curran, S.; Blau, W.; Weldon, D. N.; Dlamesiere, M.; Draper, S.; Zandbergen, H. *Chem. Phys. Lett.* **1994**, *221*, 53.
(17) Eklund, P. C.; Holden, J. M.; Jishi, R. A. *Carbon* **1995**, *33*, 959.
(18) Tuinstra, F.; Koenig, J. L. *J. Chem. Phys.* **1970**, *53*, 1126.

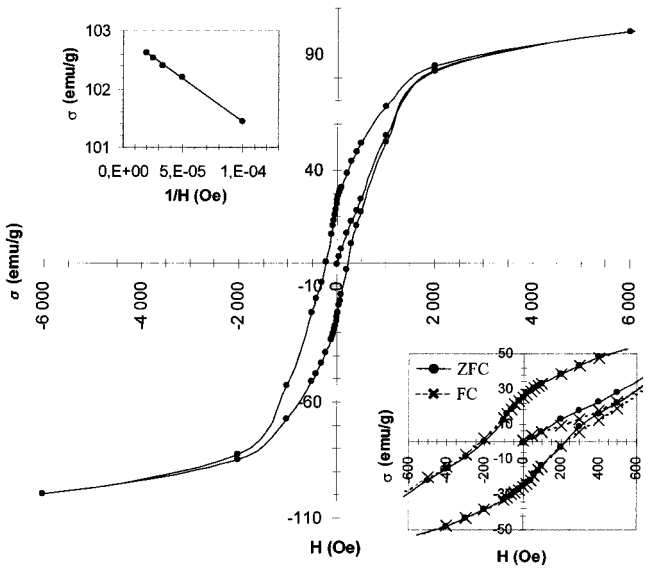

Figure 4. (a) Hysteresis loop recorded at 10 K. (b) Magnetization calculated by infinite field extrapolation from the experimental data. (c) Comparison of hysteresis loops with (FC) or without (ZFC) field cooling.

size may also explain why no (002) graphite-like reflection was observed by XRD. No signal was recorded within the carbon nanotubes RBM range (100−300 cm^{-1}, not shown), confirming that SWNTs were present only in a very small proportion in the sample. The two other peaks at high wavenumber are assigned to second-order ones (the peak at 2679 cm^{-1} could correspond to the first overtone of the D peak at 1342 cm^{-1} and the one at 2928 cm^{-1} would be close to a combination mode (1342 + 1588 cm^{-1}), expected in graphite[19]). The peaks observed at 1085 and 1124 cm^{-1} have not been identified but come neither from the starting SSI−MgO nor from any cobalt oxide. Similar peaks were however observed with crystalline graphites.[15]

Static magnetic susceptibilities were measured in the temperature range 10−300 K and with fields up to 50 kOe. The hysteresis loop at 10 K (Figure 4a) showed a coercivity of about 200 Oe. The magnetization, σ_s = 102.9 emu/g, was calculated from the experimental data by the use of an extrapolation from the infinite field (Figure 4b). Assuming on the first hand that the magnetic properties of the sample are only due to pure metallic cobalt, and on the second hand that the particle size distribution is sufficiently narrow, we deduced the percentage of metallic Co in the sample. Using the theoretical value (σ_{theo} = 162.5 emu/g), we get a mean percentage of 63.32 wt %. This value is close to that deduced from the elemental analysis (72.7 wt %) and can be considered in agreement with it, taking into account that the small difference could arise from at least two factors enumerated here: (i) the theoretical magnetization (162.5 emu/g) is calculated at 0 K compared to our 10 K experimental conditions, and (ii) it has been shown that surrounding species, especially electron donors, could strongly change the magnetization value by interacting with the surface metallic atoms.[20,21] The carbon atoms π-shell could thus be responsible for our lower experimental value.

As mentioned in the Introduction, the mean drawback of metallic particles is the reaction with surrounding oxygen molecules. In the case of Co particles, it is well-known that a metallic particle embedded in an oxide layer (CoO) exhibits an exchange anisotropy.[22] This latter can be shown by the use of a field cooling measurement: if any CoO was to be present in the sample, the hysteresis loops of the material would be shifted along the abscissa when measured during cooling with (FC) or without (ZFC) magnetic field.[22] The temperature dependence of the static susceptibility was investigated by cooling the sample with an external applied field, the hysteresis loop was then collected at low temperature. The comparison of the hysteresis loops with or without field cooling (Figure 4c) showed no shift at all. This indicates the absence of CoO around the Co nanoparticles. This result demonstrates once again that the Co nanoparticles surrounded by graphitic shells are protected from oxidation.

The coercivity measured for the carbon-encapsulated Co nanoparticles (200 Oe) is higher than that of bulk Co (typically tenths of oersteds), but in the same range than the coercivity measured for Co nanowires[23] (150−680 Oe). The enhanced coercivity can be explained by the small particle size (within the 5−15 nm range), because in the case of (fcc)-Co, the single domain size is ca. 10 nm. Similar size and morphology effects have also been observed in the case of other magnetic transition metals such as Ni[23] and Fe.[24]

Elemental mapping by energy-filtered imaging was used to image separately the carbon and the cobalt, to be able to make a clear distinction between empty and Co-filled carbon shells. Parts a−d of Figure 5 show a typical FEGTEM image of the sample, along with elemental maps for C and Co. The Co nanoparticles diameters are within the 5−15 nm range and the number of encapsulating concentric carbon shells is between 2 and 12. Empty carbon capsules are indicated by white arrows on the carbon elemental map (Figure 5a). This is shown by comparison with the Co elemental map (Figure 5b) and even more clearly in Figure 5c which shows a composite image obtained by superimposing the elemental maps for C and Co. This is also in very good agreement with the FEGTEM image (Figure 5d). To confirm the presence of Co inside the carbon capsules, a line scan analysis was performed across a selected nanoparticle, indicated by a black arrow on the top of Figure 5d. The corresponding line-scan across the nanoparticle (Figure 5e) reveals that the C and Co concentration profiles are in good agreement with what can be expected for a carbon encapsulated Co nanoparticle. The superposition over the corresponding HRTEM image makes the comparison easier. Distances are measured in nanometers, from the center of the nanoparticle. The encapsulated Co is therefore efficiently

(19) Holden, J. M.; Zhou, P.; Bi, X. X.; Eklund, P. C.; Bandow, S.; Jishi, R. A.; Chowdhury, K. D.; Dresselhaus, G.; Dresselhaus, M. S. *Chem. Phys. Lett.* **1994**, *220*, 186.

(20) Van Leeuwen, D. A.; van Ruitenbek, J. M.; de Jongh, L. J.; Ceriotti, A.; Pacchioni, G.; Häberlen, O. D.; Rösch, N. *Phys. Rev. Lett.* **1994**, *73*, 1432.

(21) Petit, C.; Taleb, A.; Pileni, M. P. *J. Phys. Chem. B* **1999**, *103*, 1805.

(22) Miklejohn, W. H.; Bean, C. P. *Phys. Rev.* **1957**, *105*, 904.

(23) Whitney, T. M.; Jiang, J. S.; Searson, P. C.; Chien, C. L. *Science* **1993**, *261*, 1316.

(24) Grobert, N.; Hsu, W. K.; Zhu, Y. Q.; Hare, J. P.; Kroto, H. W.; Terrones, M.; Terrones, H.; Redlich, Ph.; Rühle, M.; Escudero, R.; Morales, F. *Appl. Phys. Lett.* **1999**, *75*, 3363.

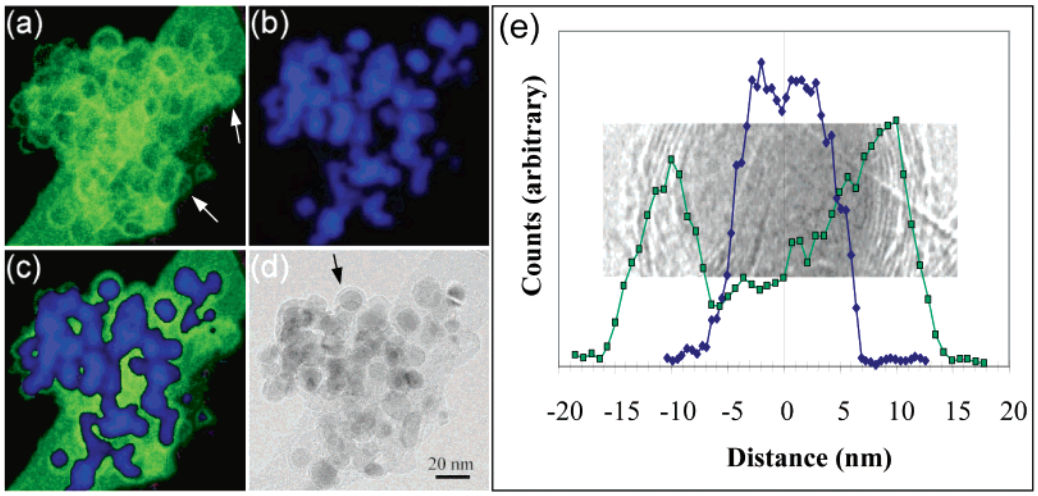

Figure 5. Energy-filtered images showing elemental maps for C (a) and Co (b). The white arrows on the image (a) point toward empty carbon shells. The superimposition of these elemental maps (c) is compared with the HRTEM image of the corresponding area (d). (e) Line scan analysis performed across a selected nanoparticle, indicated by a black arrow on Figure 4d, revealing that the C and Co concentration profiles are in good agreement with the superimposed corresponding HRTEM image.

protected from any chemical attack and, in particular, from air oxidation.

Many mechanisms have been proposed to explain the formation of CNTs by the decomposition of hydrocarbons on metal particles.[25] The key point has been shown to be the particle size, because it effectively regulates the CNT diameter.[11,26−27] The main problem is to control the particle size at temperatures generally above 700 °C at which coalescence is likely to happen readily because of enhanced surface diffusion. The use of a solid solution-based catalyst allows us to generate the nanoparticles in situ and thus to make them available for the catalytic decomposition of the hydrocarbon immediately which means that the nanoparticles can be kept to a small particle size range. In our study, the first step is the simultaneous selective reduction of CoO to Co metal and the decomposition of the CH_4 at the surface of the Co nanoparticles, leading to the likely formation of a (Co, C) alloy whose carbon content is increasing with time. Because the CH_4 flow rate is quite low, we believe that insufficient carbon is dissolved in the Co nanoparticles to reach the saturation point at which precipitation of solid carbon around the nanoparticles would begin, leading to the formation of CNTs, carbon nanofibers, or carbon shells, depending on the particle size.[28,29] This is confirmed experimentally by the very low amount of CNTs observed in our sample as well as by the absence of any carbon nanofiber.

Our results may be compared with those of Zhong et al.[30] who obtained large Co nanoparticles within the 50−200 nm range using a two-step reaction process, involving initially the reduction of their catalyst in H_2 followed by reaction with CH_4. Their work resulted in the formation of big Co particles, which then led to a mixture of defected MWNTs and large carbon-encapsulated Co nanoparticles. We propose that under our experimental conditions, the encapsulation of the Co nanoparticles is likely to take place during the cooling step because the solubility of C in Co decreases drastically when the temperature drops to room temperature. This is supported by the experimental TEM observations, which showed generally the absence of voids within the carbon shells between the metal and the first graphitic layer. Cobalt carbides that may have formed are actually metastable and would decompose to give Co and carbon. As described previously, we observed no correlation between the number of concentric carbon shells surrounding the Co nanoparticles and the particle size. Because the surface/volume ratio is decreasing rapidly as the particle radius increases, we would expect the carbon content to decrease also, thus leading during the cooling step to an increasing number of concentric carbon shells as the particle diameter decreases. The experimental observation of a few CNTs, mainly SWNTs, is in good agreement with the following hypothesis: only particles with a small enough diameter (below 3 nm) would have been likely to contain enough carbon to reach the saturation point (only because of the low CH_4 flow rate), allowing the nucleation and then growth of a CNT. The observation of small particles (around 5 nm in diameter) with only two or three concentric carbon shells could be explained by their late formation during the reduction process. This may be the reason we cannot find any striking correlation between the particle size and the number of concentric carbon shells.

Conclusion

We have described a new method for the preparation of carbon-encapsulated (fcc)-Co nanoparticles with diameters within the 5−15 nm range. The new concept of the solid solution impregnated support has allowed us to obtain a carbon yield more than 50 wt % compared to the Co weight, this carbon being mainly present in the form of carbon shells surrounding the Co nanopar-

(25) Laurent, Ch.; Flahaut, E.; Peigney, A.; Rousset, A. *New J. Chem.* **1998**, 1229.
(26) Amelinckx, S.; Zhang, X. B.; Bernaerts, D.; Zhang, X. F.; Ivanov, V.; Nagy, J. B. *Science* **1995**, *265*, 635.
(27) Dai, H.; Rinzler, A. G.; Nikolaev, P.; Thess, A.; Colbert, D. T.; Smalley, R. E. *Chem. Phys. Lett.* **1996**, *260*, 471.
(28) Hafner, J. H.; Bronikowski, M. J.; Azamian, B. R.; Nikolaev, P.; Rinzler, A. G.; Colbert, D. T.; Smith, K. A.; Smalley, R. E. *Chem. Phys. Lett.* **1998**, *296*, 195.
(29) Flahaut, E. D. Philos. Thesis, University of Toulouse III, Toulouse, France, 1999.
(30) Zhong, Z.; Chen, H.; Tang, S.; Ding, J.; Lin, J.; Tan, K. L. *Chem. Phys. Lett.* **2000**, *330*, 41.

ticles. We have proposed a mechanism for the formation of these carbon-encapsulated Co nanoparticles, and their stability vs air oxidation and HCl treatment at room temperature has been demonstrated. Magnetic measurements confirm that the carbon-encapsulated Co nanoparticles are protected against oxidation and remain metallic. With a narrowing of the diameter distribution, the 2D organization (i.e., a self-assembling method) of such magnetic nanoparticles could be a step forward in the realization of high-density recording media.

Acknowledgment. We thank DARPA through DARPA Grant No. MDA 972-97-1-0003 and the Army Research Office Grant No. DAAD19-99-1-0001. Financial support was also provided by the donors of the the Petroleum Research Fund, administered by the American Chemical Society, through Grant No. 33765-ACS, and by the EPSRC (Grants Nos. GR/L59238 and GR/L22324).

CM011287H